In Situ Study of Li Intercalation into Highly Crystalline Graphitic Flakes of Varying Thicknesses

Jianli Zou[1], Christopher Sole[1], Nicholas E. Drewett[1], Matěj Velický[2] and Laurence J. Hardwick[1*]

[1]Stephenson Institute for Renewable Energy, Department of Chemistry, University of Liverpool, L69 7ZD, UK

[2]School of Chemistry, University of Manchester, Oxford Road, Manchester, M13 9PL, UK

Corresponding Author

* Email: hardwick@liverpool.ac.uk

Stephenson Institute for Renewable Energy, Department of Chemistry, University of Liverpool, L69 7ZD, UK

Abstract

An *in situ* Raman spectroelectrochemical study of Li intercalation into graphite flakes with different thicknesses ranging from 1.7 nm (3 graphene layers) to 61 nm (ca. 178 layers) is presented. The lithiation behavior of these flakes was compared to commercial microcrystalline graphite with a typical flake thickness of ca. 100 nm. Li intercalation into the graphitic flakes was observed under potential control via *in situ* optical microscopy and Raman spectroscopy. As graphite flakes decreased in thickness, a Raman response indicative of increased tensile strain along the graphene sheet was observed during the early stages of intercalation. A progressively negative wavenumber shift of the interior and bounding modes of the split G band (E_{2g2}(i) and E_{2g2}(b)) is interpreted as a weakening of the C-C bonding. Raman spectra of Li intercalation into thin graphitic flakes are presented and discussed in the context of implications for Li-ion battery applications, given intercalation induced strain may accelerate carbon negative electrode aging and reduce long-term cycle life.

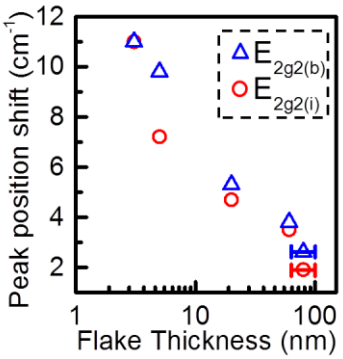

Rechargeable Lithium-ion batteries represent the leading energy storage technology solution for many applications such as portable electronics, power tools and electric vehicles, and represent strong considerations for various grid storage systems.[1,2] In commercial Li-ion devices, bulk graphite is the most widely used anode material due to its cost-effective performance. Li intercalation into graphite proceeds via a series of staged graphite intercalation compounds (GICs), classified by stage index, *n*, whereby *n* represents the number of graphene layers separating intercalated ions. The first and/or second order Raman spectra of graphitic carbons during the first lithiation and delithiation has been investigated in a typical lithium-ion battery electrolyte by ourselves[3–5] and others[6,7] in order to understand Li intercalation into practical carbon electrodes. *In situ* Raman spectroscopic measurements under potential control enable the probing of the graphitic negative electrode during ion insertion and extraction. Experimental results reveal the typical staging formation on different regions of the electrode surface from the splitting of the G band (1580 cm^{-1}) into a doublet band.[7] The lower (E_{2g2}(i)) and upper (E_{2g2}(b)) frequency components are correspondingly associated with carbon-atom vibrations in interior graphite layers (not adjacent to the intercalate layer planes) and in bounding graphite layers (adjacent to the intercalate planes). The split in the G (E_{2g2}) mode upon intercalation occurs primarily from changes in symmetry at the boundary layer, and secondarily from the electronic effects of the intercalate molecule. The E_{2g2}(i) band disappears for stage 1 and 2, where no graphite interior layer exists.[7]

Recent research interest in graphene has led to a variety of studies on the chemical doping of single layer and intercalation of guest species into few-layer graphene systems. For example, *in situ* Raman spectroscopy has been used to monitor the doping (intercalation) of single-layer (bilayer) graphene with rubidium vapor.[8] In another study, the intercalation of ferric chloride ($FeCl_3$) into graphite flakes consisting of 2-4 graphene layers has also been characterized by Raman

spectroscopy.[9] Nevertheless, despite the fact that Li-GICs have been extensively studied since the 1970s,[10–16] the difference in the electrochemical lithiation process with various graphene layer thicknesses is still not well understood. A number of authors have recently applied Raman spectroscopy to understand the lithiation mechanism for graphenic materials. Pollak et al.[17] studied the interaction of Li with few layer graphene and concluded that the process seems to resemble that of bulk graphite. However, recent work[18] suggested that Li intercalation into few layers of graphene showed a strong dependence on the number of graphene layers, as measured via stationary voltammetry.

Herein we present an *in situ* Raman spectroelectrochemical study of Li intercalation into edges of highly crystalline graphite with different thicknesses ranging from 1.7 nm (3 graphene layers) to 61 nm (ca. 178 layers). The lithiation behavior of these flakes was compared to commercial microcrystalline graphite (60-100 nm thick) and it was observed that with decreasing flake thickness, the downshift of both E_{2g2}(i) and E_{2g2}(b) bands increases, which is indicative of additional tensile strain upon the graphene sheets during ion insertion.

Highly crystalline natural graphite flakes (NGS Naturgraphit GmbH) were mechanically exfoliated onto a borosilicate glass cover slide using the 'Scotch tape method'.[19,20] Flakes were selected according to the following requirements: ideal flakes should possess a thin flat region of several square micrometers area to allow facile Raman analysis, whilst the whole flake should be bigger than a few hundred micrometers and thick enough (> 500 nm) at one edge to facilitate electronic connection using silver epoxy. Figure 1a illustrates the sample fabrication process and its formation into an electrode for the *in situ* spectroelectrochemical Raman cell. Graphitic flake thicknesses were determined by atomic force microscopy (AFM). Silver epoxy was used to make an electronic connection between the graphitic flake and the copper current collector, leaving the area of interest pristine. The position of the flake was aligned to coincide with the small aperture (ca. 1 mm diameter) made in the center of the copper current collector for direct optical observation. The silver epoxy contact was positioned facing the glass window in order to minimize possible contact with the electrolyte. The graphite flake electrode was assembled in an EL-CELL® spectroelectrochemical Raman cell (ECC-Opto-Std). Figure 1b shows the simplified version of the configuration of the test cell, with graphite flake acting as working electrode and Li metal as counter electrode. A free standing microcrystalline flake graphite electrode was prepared as described previously (IMERYS, SFG6, typical flake thickness estimated from SEM images of the microcrystalline graphite, is between 60-100 nm, Figure S1)[3] 1 M $LiPF_6$ in 1:1 w/w ethylene carbonate/dimethyl carbonate (BASF) was used as electrolyte. Cyclic voltammetry was performed using a potentiostat (Biologic) to induce electrochemical intercalation of the graphite samples. Initially, the cell was discharged at 0.02 mV/s from open circuit voltage (OCV) to 1.2 V (vs. Li^+/Li), then a slower rate of 0.005 mV/s was employed between 1.2 V to 0.005 V vs. Li^+/Li, whilst Raman spectra were collected at room temperature (ca. 23 ^oC) (Renishaw *inVia*, laser wavelength 532 nm,

< 19 kW/cm^2). Due to the slow scan rate employed, changes during lithiation of the graphite sample were occurring on the timescale of the spectral acquisitions, allowing spectra to be collected at a quasi-equilibrium state. Furthermore, unless otherwise stated all Raman measurements have been taken a few micrometers from the flake edge to reduce/mitigate differences arising from inhomogeneous Li diffusion induced by defects and grain boundaries within the crystalline flake. The successful electronic connection to the graphitic flakes was confirmed by the observation of Li intercalation though optical visualization of the well-documented phenomena of color changes in the flake and corresponding Raman spectra, relating to staged Li insertion (Figure S2).[21–24]

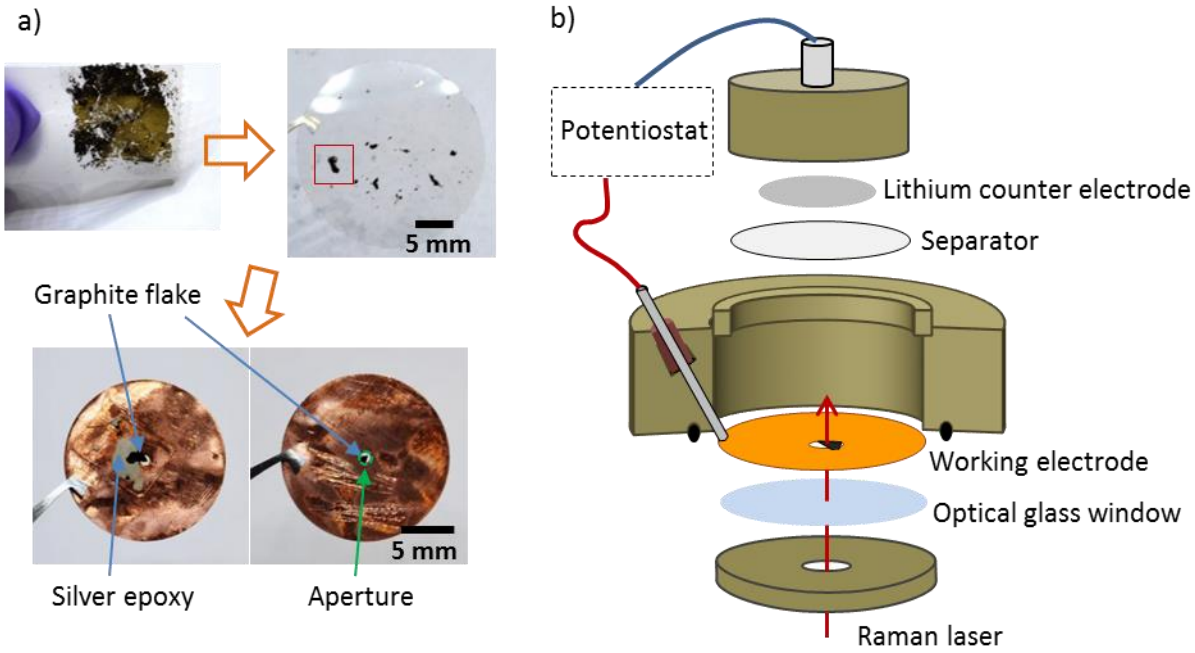

Figure 1. Schematic illustration of the assembly of graphite flake into the *in situ* spectroelectrochemical Raman cell. a) Graphite flakes were mechanically exfoliated onto a borosilicate glass cover slide. A single graphite flake was selected, isolated using a diamond tipped glass cutter and connected to a copper current collector using silver epoxy, ensuring that the area

of interest was aligned with the aperture in the center for direct observation. b) The copper-glass sandwich with the contacted graphite flake (working electrode) was assembled in an EL-CELL® electrochemical test cell (ECC-Opto-Std) with the silver epoxy on the opposite side of the current collector to the electrolyte-impregnated separator.

Figure 2 shows the AFM images, height profile and Raman characterization of three representative graphite flakes used in this study. The thicknesses were 1.7 nm (Figure 2a), 3.8 nm (Figure 2b), and 20 nm (Figure 2c), corresponding to 3 graphene layers, 9 graphene layers and ~56 graphene layers respectively. Raman spectroscopy is a powerful analytical tool for study of both GICs and few layer graphene, and it is a key tool to probe the physical and electronic properties in graphene-based materials.[10,25–27] Analysis of the two main signals in the Raman spectra, the G band around 1582 cm^{-1} and the dispersive double resonance peak in the range between 2600 and 2700 cm^{-1} (2D band), offers detailed information; e.g. it allows determination of the number of graphene layers, induced strain in the structure, and charging.[28] The Raman spectra of all three graphite flakes exhibit two intense peaks: G band at ~1582 cm^{-1} and 2D band at ~2700 cm^{-1} for the 3 layer sample and ~2718 cm^{-1} for other thicker flakes (Figure 2d-f). The absence of a D band at ~ 1350 cm^{-1} indicates the very low defect density in our mechanically exfoliated natural graphite samples.

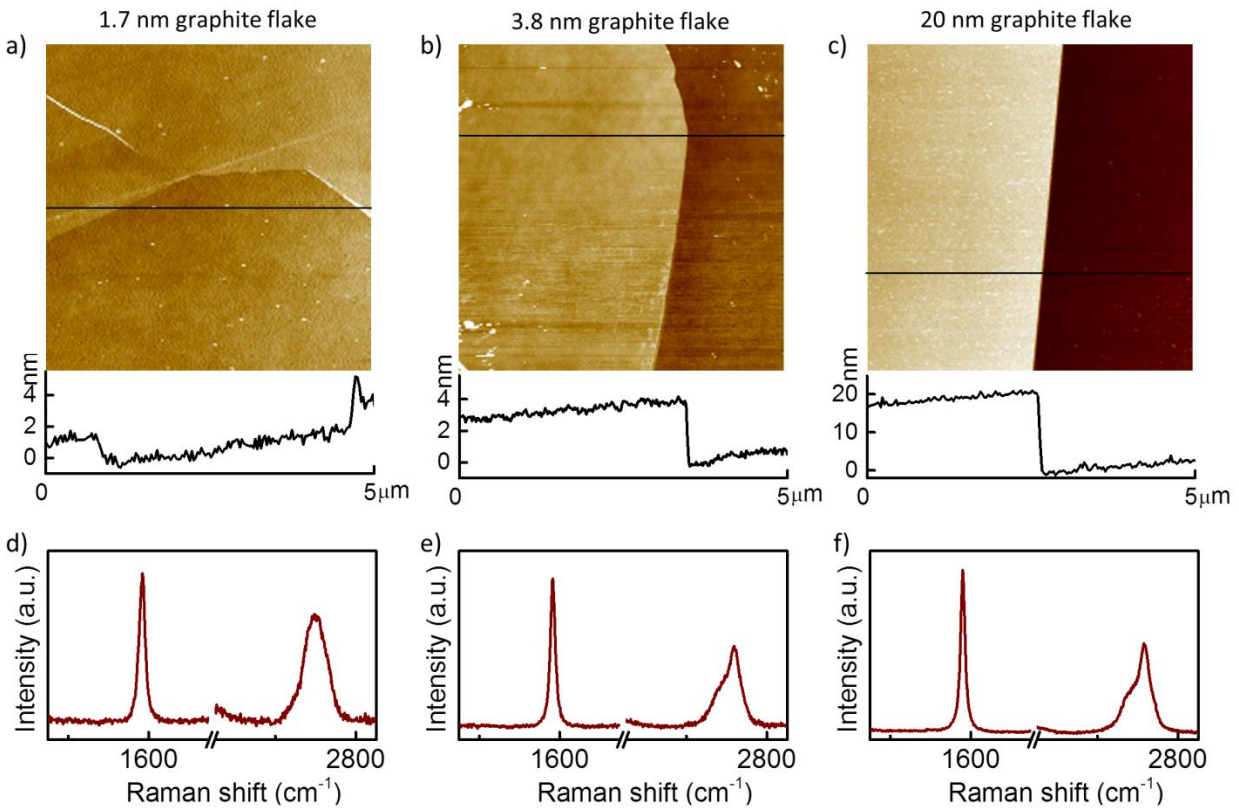

Figure 2. Characterization of graphite flakes by AFM and Raman spectroscopy. a-c) AFM images and the height profiles of three graphite flakes with the thickness of 1.7 nm (3 graphene layers), 3.8 nm (9 graphene layers), and 20 nm (ca. 56 graphene layers). d-f) Corresponding Raman spectra of the graphite flakes shown in a), b) and c).

Figure 3 shows the *in situ* Raman spectra of microcrystalline flake graphite and graphite flakes with three different thicknesses (1.7 nm, 3.8 nm and 20 nm) during lithiation. During Li insertion for all samples, the 2D band was observed to shift to lower wavenumbers, accompanied by the decrease of intensity, as has previously been recorded.[3] The intercalation behavior of 20 nm and 3.8 nm thick graphite flakes display similar characteristics to that of microcrystalline flake graphite. A clear split of the G band to E_{2g2}(i) and E_{2g2}(b) modes at around 0.22 V was preceded by an upshift in G band frequency. The splitting of the G band can be interpreted as the graphene layers

next to intercalate Li layers being differentiated from those adjacent to empty galleries, according to the *nearest layer* model of Nemanich and Solin.[16]

In contrast the 1.7 nm (3 layer) graphitic edge flake showed rather different behavior, as a definitive G band split was not observed during lithiation (although this was difficult to fully resolve due to the low initial OCV intensity signal as shown in Figure S3). The 2D band vanished into the background noise at a relatively high potential (not detectable by 0.19 V), after an initial measurable downshift from 2718 to 2704 cm^{-1}. Within the 3 graphene layers, formation of stage 3 and stage 4 during lithiation is not possible, so it can be concluded from the Raman data that lithiation occurs directly *via* dilute stage 1 GIC to stage 1. In contrast, splitting of the G band was observed in a previous study whereby a 3 graphene layer sample was chemically doped by NO_2 adsorption.[29] In this case G peak splitting arose as only the surface layers were doped, leaving the interior layers undoped. In Figure 3d no obvious splitting is observed as all three layers are adjacent to Li ions, suggesting that during the intercalation process Li ions are distributed in both available interlayer spaces. It should be noted that with respect to all single flake measurements reported in this study, it is not possible to completely distinguish whether the Li ions are inserting directly at the studied flake edge/electrolyte interface or have diffused into the thinner flake from being initially intercalated into the bulk graphite crystal.

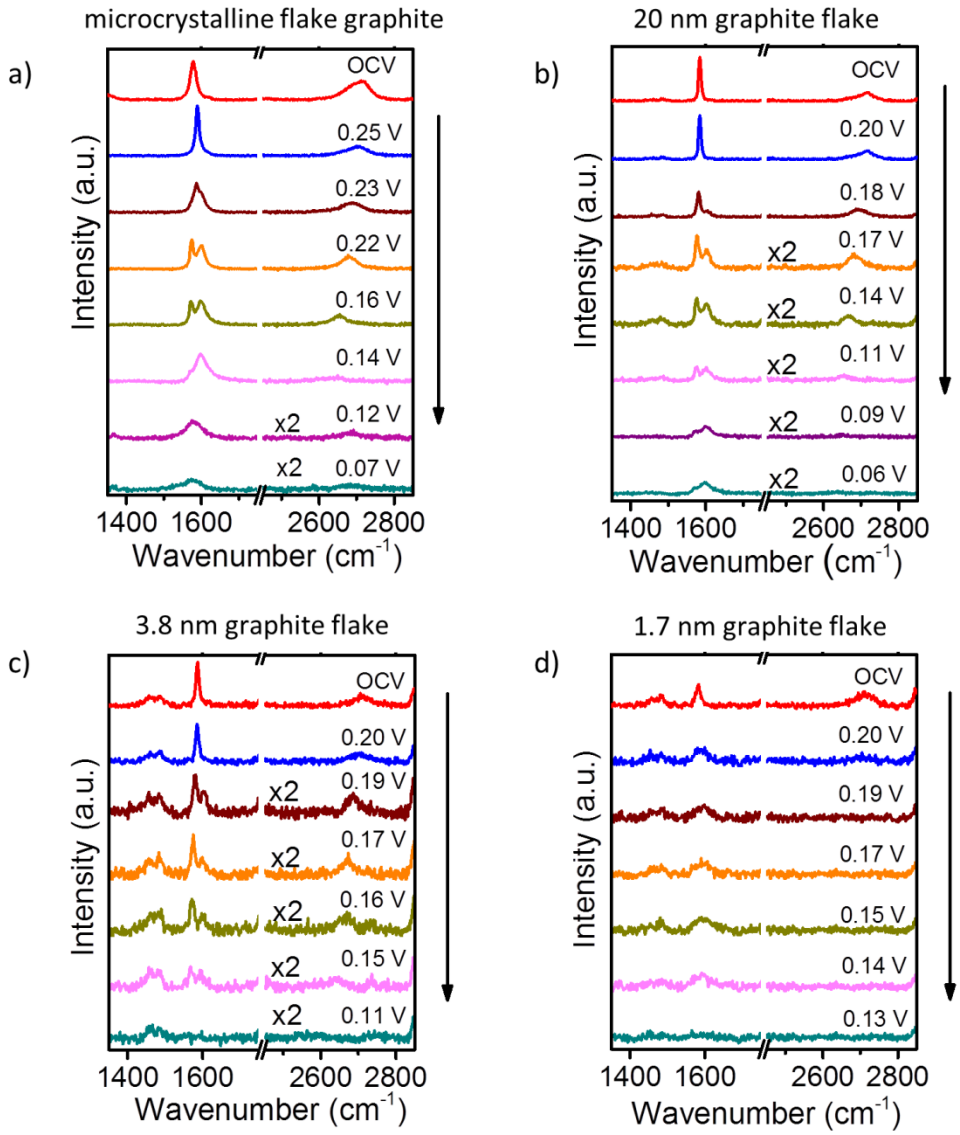

Figure 3. Raman spectra during lithiation of a) microcrystalline flake graphite with ca. 60-100 nm thickness, and graphite flakes with b) 20 nm (ca. 56 graphene layers), c) 3.8 nm (9 graphene layers) and d) 1.7 nm (3 graphene layers) thicknesses. OCV was ca. 2.9 V, all potentials quoted measured vs. Li^+/Li (see Figure S3 for the comparison of G peak intensity at OCV).

In order to further compare the results, the peak position of the G band was plotted versus potential in Figure 4 and Figure S4. All samples experienced an upshift in G band frequency before the

splitting occurred as previously observed below ca. 0.2 V vs Li^+/Li.[3,24,30] This upshift can be understood by considering the doping effect during the dilute stage 1 phase in all samples. The stiffening of the E_{2g2} phonon with doping has been previously explained by an increase in the force constants of in-plane C-C bonds, whilst similar behavior has been observed in single layer graphene (SLG).[31] Interestingly, the upshift is more prominent for the microcrystalline flake graphite compared to all single flake samples. Upshifts of the G band (ca. 10 cm^{-1}) have been observed previously by ourselves[3] and Shi et al.[30] Dilute stage 1 formation is responsible for between 4-7 % of the theoretical capacity of graphite (~20 mAh/g vs. 372 mAh/g),[11] thus the lower doping in this region for our single flake samples suggests that the proportion of Li insertion during the dilute stage 1 GIC phase decreases as you reduce the flake thickness of graphite particles.

The G band then splits into the E_{2g2}(i) peak at lower wavenumber and the E_{2g2}(b) peak at higher wavenumber indicated by the dashed line in Figure 4. Significantly, as the intercalation progressed both E_{2g2}(i) and E_{2g2}(b) downshifted, showing the trend whereby the thinner the flake, the steeper the slope of the shift from 0.2 V vs. Li^+/Li onwards. The downshift in the band position can be considered to be the result of biaxial tensile strain as has been previously observed.[27,32] Electron doping of the graphene sheets causes occupation of the π^* anti-bonding band, which produces a weakening and elongation of the intralayer C-C bonds within the graphene sheets.[33–35]

Figure 4d compares the Raman peak shift of the split G band for graphite flakes of different thicknesses (see Figure S4 for peak position of G band during intercalation for 61 nm and 5 nm thick graphite flakes). E_{2g2}(b) position shifts of up to 11 cm^{-1} for the 3.8 nm flake and down to 2.6 cm^{-1} for the microcrystalline flake graphite corresponding to the stage 4 to stage 3 transition. The shift in the G peak position ($\Delta\omega_{E_{2g2}}$) with biaxial tensile strain (ε) is given by:

$$\Delta\omega_{E_{2g2}} = -2\omega^0_{E_{2g2}}\gamma_{E_{2g2}}\varepsilon \quad (1)$$

where $\omega^0_{E_{2g2}}$ is the Raman frequency of unstrained graphene and $\gamma_{E_{2g2}}$ the Grüneisen parameter. Mohiuddin et al.[32] have determined $\gamma_{E_{2g2}}$= 1.99 causing a -63 cm^{-1} shift in G band position per % biaxial strain. This shift is constant regardless of flake thickness; therefore the biaxial strain in the microcrystalline flake graphite and 3.8 nm flake can be calculated as 0.04 % and 0.17 % respectively. The data therefore suggests an increase in the strain as the thickness of flakes decrease, meaning the increase in C-C bond lengths is greater with decreasing flake thickness as shown in Figure 4d. Previous measurements have shown the C-C bond length increases by ~ 1.0 % upon lithiation of bulk graphite to LiC_6, with C-C bond lengths of 1.421 Å and 1.435 Å respectively.[36,37] At first glance the calculated values for the increased tensile strain and bond length increase do not appear to be too remarkable, and may not seem to be relevant for technological applications. However, Li-ion battery graphitic anodes have shown an increase of graphitic disorder (as indicated by an increase of D band intensity with respect to the G band) after repeated shallow cycling, even with the assumption of 0.04 % increase in tensile strain.[38] The surface of the graphite anode undergoes gradual structural degradation upon cycling and this effect has been reported to occur generally in all graphitic carbons.[38-40] During the aging of the anode, a damaged graphite surface consumes the cycleable Li inventory via further solid electrolyte interphase formation on the freshly exposed carbon surface.[41] Thereby an increase to 0.17 % biaxial tensile strain could lead to a more rapid graphitic disordering during repeated Li insertion/extraction cycles, suggesting there may be an optimum range of flake thickness for long lifetime graphitic Li-ion anodes.

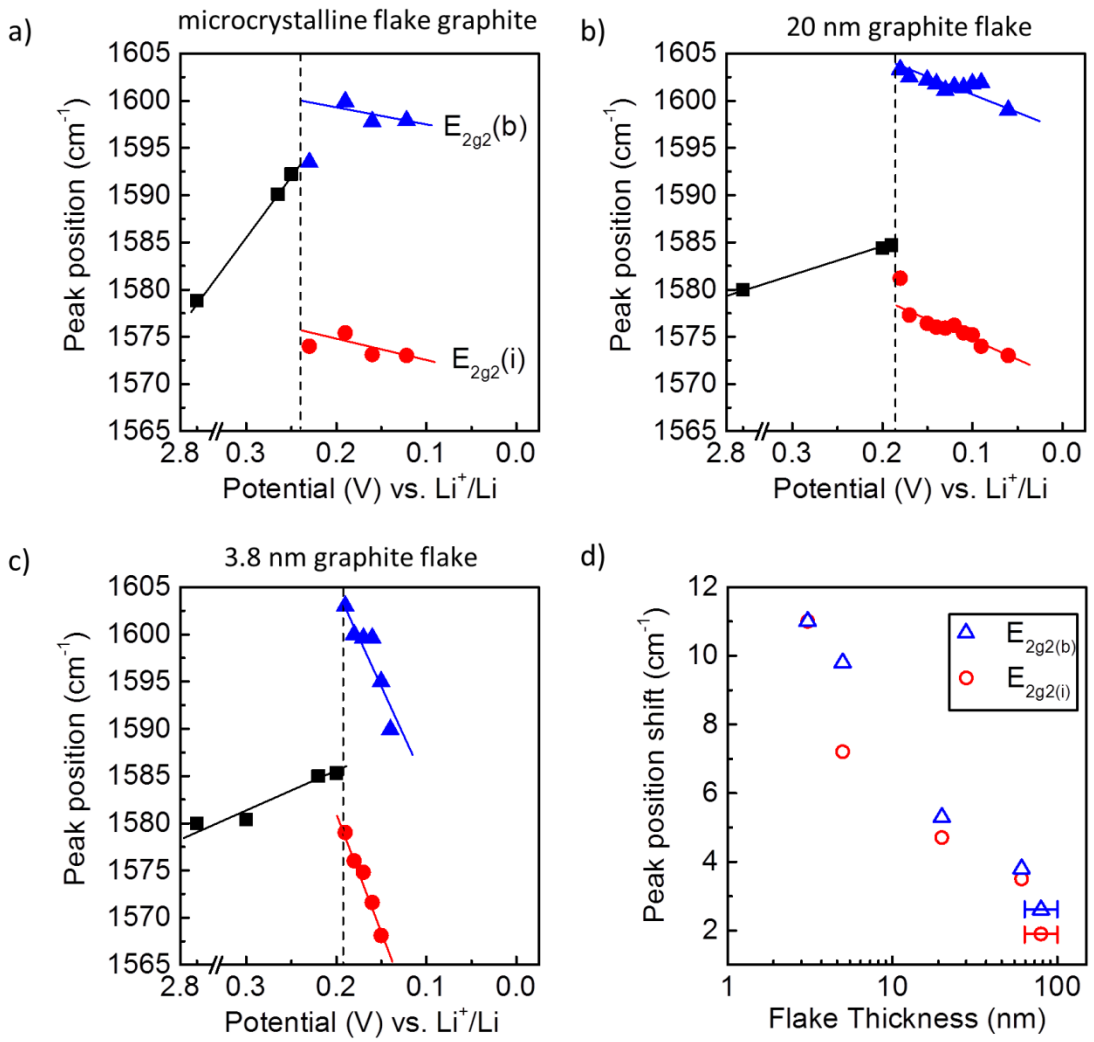

Figure 4. The peak position of the G band during intercalation for a) microcrystalline flake graphite, b) 20 nm graphite flake and c) 3.8 nm graphite flake. The dashed line indicates when splitting occurred. d) The comparison of the Raman peak shift of the split G band for graphite flakes with different thicknesses.

Analysis of the Raman spectra for intercalation into the 3 layer graphene flake provides further evidence that the G band position is a sum of the competing processes of doping induced upshift and strain induced downshift (Figure 5). The initial upshift of the G band position is again observed, concurrent with the formation of dilute stage 1, which continues until ~ 0.15 V when it begins

downshifting and then loses observable intensity. The lack of obvious splitting, as discussed earlier, suggests a bypassing of the conventional stage 4 and stage 3 formation, and continuation of dilute stage 1 until the later stages of intercalation. Significantly, the similar trend of G band position suggests the competing influence of upshift caused primarily by electron doping and subsequent downshift due to significant biaxial strain. This is highlighted in Figure 5 where the mean G band position of the 9 layer graphite flake is plotted alongside the G band of 3 layer graphite sample. The trend of arithmetic mean values of E_{2g2}(i) and E_{2g2}(b) peak position showed a close resemblance to the G band position in the 3 layer graphite flake. This similar trend is also shown in other thickness flakes (supporting information Figure S5).

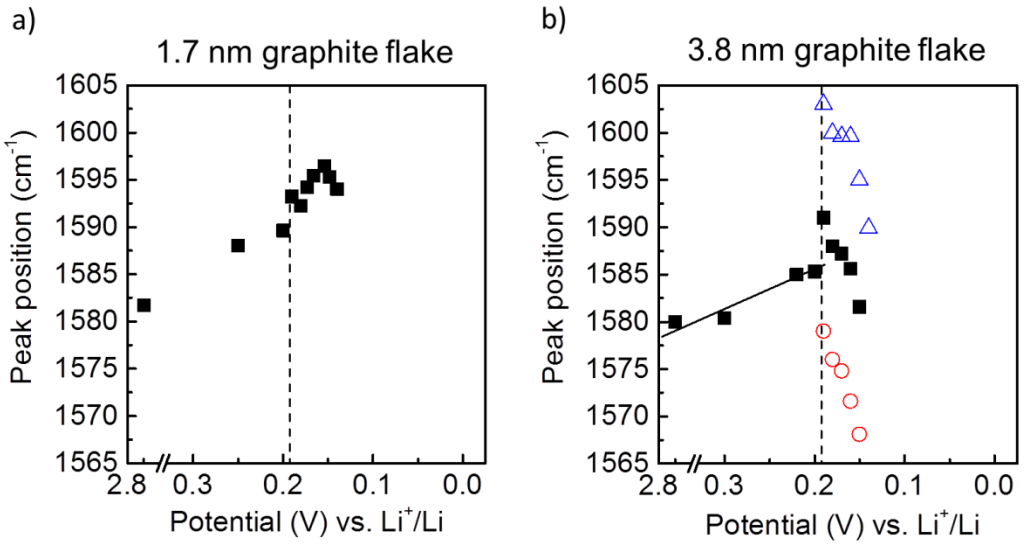

Figure 5. The comparison of G peak position of a) 1.7 nm (3 graphene layers) and b) 3.8 nm (9 graphene layers) graphite flakes during lithiation. The blue and red cycles in b) are the real data of $E_{2g2(i)}$ and $E_{2g2(b)}$ and the solid squares (after the dashed line) represent the arithmetic mean value of both E_{2g2} band. The dash line in a) indicates where G peak splits in b).

The 2D band is known to be a more sensitive indicator of strain than the G band.[25,32] Similarly to previous studies,[3,28] we observe a clear downshift of the 2D band followed by a loss of all observable intensity. Figure 6 shows the shift in 2D band position, from the first spectra that a split G peak is observed for each sample, until the last spectra in which the 2D band remains visible. For samples thicker than 5 nm a large downshift of the 2D band is observed (ca. 40 cm^{-1}), yet below 10 nm thickness the 2D band shift is significantly less. The downshift has previously been ascribed to a combination of doping and tensile strain, suggesting one of these factors is lessened for the thinner single flake samples. However, previous studies have shown electron doping also causes a rapid decrease in 2D band intensity.[42,43] Due to the reduced signal to background intensity of the thinner single flake samples (Figure S3), this causes the disappearance of the 2D band at earlier potentials (Figure 3) which results in smaller observed 2D band shifts. Therefore, although a difference in 2D band behavior with flake thickness is observed, it is not possible to draw strong conclusions regarding strain and doping to support those from the reported G band analysis.

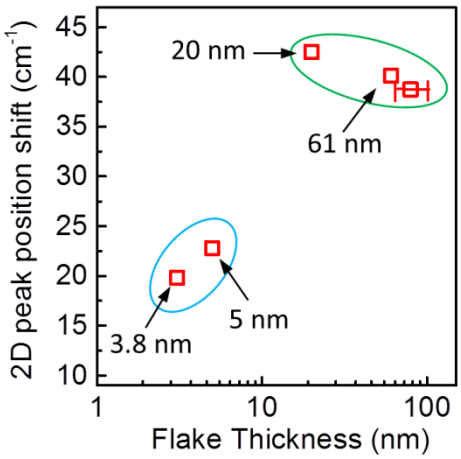

Figure 6. The 2D peak position shift from the first spectra that a split G peak is observed, until the last spectra in which the 2D band remains detectable above the signal noise for samples of 3.8 nm

(9 graphene layer), 5 nm (ca. 13 graphene layers), 20 nm (ca. 56 graphene layers), 61 nm (ca. 178 graphene layers) and microcrystalline flake graphite (ca. 60-100 nm) during lithiation.

In summary, electrochemical lithiation in large graphitic flakes with different thicknesses ranging from ca. 100 nm down to three graphene layers thick, have been systemically studied via *in situ* Raman spectroscopy. With decreasing flake thickness, a Raman response indicative of increased tensile strain during the early stages of Li intercalation, when compared to thicker (60-100 nm) commercial microcrystalline graphite flakes, was detected. As intercalation induced strain is one of the causes of battery capacity fade during long-term cycling, due to gradual disordering of graphitic anodes, this study highlights the possible increase of the rate graphite degradation if thinner flakes are used within commercial Li-ion cells. Further analysis is required to clarify the impact on the aging via multiple Li insertion/extraction cycles of graphitic negative electrodes (anodes) consisting of flakes thinner than 20 nm.

ASSOCIATED CONTENT

Supporting Information Available: Preparation of microcrystalline flake graphite electrode method, SEM image of microcrystalline flake graphite, intercalation dynamics discussion and optical microscopy images, comparison of absolute Raman intensity of samples at OCV, G band position shift for 61 nm and 5 nm thick graphite flake, comparison of position of split G band arithmetic mean for all samples. This material is available free of charge via the Internet http://pubs.acs.org.

AUTHOR INFORMATION

Notes

The authors declare no competing financial interest.

ACKNOWLEDGMENTS

We acknowledge the Engineering and Physical Sciences Research Council (EPSRC) for the funding of this research under grant number EP/K016954.

REFERENCES

(1) Tarascon, J. M.; Armand, M. Issues and Challenges Facing Rechargeable Lithium Batteries. *Nature* **2001**, *414*, 359–367.

(2) Goodenough, J. B.; Park, K.-S. The Li-Ion Rechargeable Battery: A Perspective. *J. Am. Chem. Soc.* **2013**, *135*, 1167–1176.

(3) Sole, C.; Drewett, N. E.; Hardwick, L. J. In Situ Raman Study of Lithium-Ion Intercalation into Microcrystalline Graphite. *Faraday Discuss.* **2014**, *172*, 223–237.

(4) Sole, C.; Drewett, N. E.; Liu, F.; Abdelkader, A. M.; Kinloch, I. A.; Hardwick, L. J. The Role of Re-Aggregation on the Performance of Electrochemically Exfoliated Many-Layer Graphene for Li-Ion Batteries. *J. Electroanal. Chem.* **2015**, *753*, 35–41.

(5) Hardwick, L. J.; Buqa, H.; Novák, P. Graphite Surface Disorder Detection Using in Situ Raman Microscopy. *Solid State Ion* **2006**,. *177*, 2801–2806.

(6) Migge, S.; Sandmann, G.; Rahner, D.; Dietz, H.; Plieth, W. Studying Lithium Intercalation into Graphite Particles via in Situ Raman Spectroscopy and Confocal Microscopy. *J. Solid State Electrochem.* **2005**, *9*, 132–137.

(7) Inaba, M.; Yoshida, H.; Ogumi, Z. In Situ Raman Study of Electrochemical Lithium Insertion into Mesocarbon Microbeads Heat-Treated at Various Temperature. *J.*

Electrochem. Soc. **1996**, *143*, 2572–2578.

(8) Parret, R.; Paillet, M.; Huntzinger, J.-R.; Nakabayashi, D.; Michel, T.; Tiberj, A.; Sauvajol, J.-L.; Zahab, A. A. In Situ Raman Probing of Graphene over a Broad Doping Range upon Rubidium Vapor Exposure. *ACS Nano* **2013**, *7*, 165–173.

(9) Zhao, W.; Tan, P. H.; Liu, J.; Ferrari, A. C. Intercalation of Few-Layer Graphite Flakes with FeCl3: Raman Determination of Fermi Level, Layer by Layer Decoupling, and Stability. *J. Am. Chem. Soc.* **2011**, *133*, 5941–5946.

(10) Dresselhaus, M. S.; Dresselhaus, G. Intercalation Compounds of Graphite. *Adv. Phys.* **2002**, *51*, 1–186.

(11) Dahn, J. R. Phase Diagram of Li_xC_6. *Phys. Rev. B* **1991**, *44*, 9170–9177.

(12) Yazami, R.; Touzain, P. A Reversible Graphite-Lithium Negative Electrode for Electrochemical Generators. *J. Power Sources* **1983**, *9*, 365–371.

(13) Yamada, Y.; Takazawa, Y.; Miyazaki, K.; Abe, T. Electrochemical Lithium Intercalation into Graphite in Dimethyl Sulfoxide-Based Electrolytes : Effect of Solvation Structure of Lithium Ion. *J. Phys. Chem. C* **2010**, *114*, 11680–11685.

(14) Yamada, Y.; Furukawa, K.; Sodeyama, K.; Kikuchi, K.; Yaegashi, M.; Tateyama, Y.; Yamada, A. Unusual Stability of Acetonitrile-Based Superconcentrated Electrolytes for Fast-Charging Lithium-Ion Batteries. *J. Am. Chem. Soc.* **2014**, *136*, 5039–5046.

(15) Yamada, Y.; Yaegashi, M.; Abe, T.; Yamada, A. A Superconcentrated Ether Electrolyte for Fast-Charging Li-Ion Batteries. *Chem. Commun.* **2013**, *49*, 11194–11196.

(16) Solin, S. A. *Graphite Intercalation Compounds*; Springer-Verlag: Berlin, Germany; 1990.

(17) Pollak, E.; Geng, B.; Jeon, K.-J.; Lucas, I. T.; Richardson, T. J.; Wang, F.; Kostecki, R. The Interaction of Li with Single-Layer and Few-Layer Graphene. *Nano Lett.* **2010**, *10*,

3386–3388.

(18) Hui, J.; Burgess, M.; Zhang, J.; Rodríguez-López, J. Layer Number Dependence of Li^+ Intercalation on Few-Layer Graphene and Electrochemical Imaging of Its Solid-Electrolyte Interphase Evolution. *ACS Nano* **2016**, *10*, 4248–4257.

(19) Novoselov, K. S.; Geim, A. K.; Morozov, S. V; Jiang, D.; Zhang, Y.; Dubonos, S. V; Grigorieva, I. V; Firsov, A. A. Electric Field Effect in Atomically Thin Carbon Films. *Science* **2004**, *306*, 666–669.

(20) Novoselov, K. S.; Jiang, D.; Schedin, F.; Booth, T. J.; Khotkevich, V. V; Morozov, S. V; Geim, A. K. Two-Dimensional Atomic Crystals. *Proc. Natl. Acad. Sci. U. S. A.* **2005**, *102*, 10451–10453.

(21) Maire, P.; Evans, A.; Kaiser, H.; Scheifele, W.; Novák, P. Colorimetric Determination of Lithium Content in Electrodes of Lithium-Ion Batteries. *J. Electrochem. Soc.* **2008**, *155* 862–865.

(22) Maire, P.; Kaiser, H.; Scheifele, W.; Novák, P. Colorimetric Determination of Lithium-Ion Mobility in Graphite Composite Electrodes. *J. Electroanal. Chem.* **2010**, *644*, 127–131.

(23) Harris, S. J.; Timmons, A.; Baker, D. R.; Monroe, C. Direct in Situ Measurements of Li Transport in Li-Ion Battery Negative Electrodes. *Chem. Phys. Lett.* **2010**, *485*, 265–274.

(24) Inaba, M.; Yoshida, H.; Ogumi, Z.; Abe, T.; Mizutani, Y.; Asano, M. In Situ Raman Study on Electrochemical Li Intercalation into Graphite. *J. Electrochem. Soc.* **1995**, *142*, 20–26.

(25) Ferrari, A. C.; Basko, D. M. Raman Spectroscopy as a Versatile Tool for Studying the Properties of Graphene. *Nat. Nanotechnol.* **2013**, *8*, 235–246.

(26) Malard, L. M.; Pimenta, M. A.; Dresselhaus, G.; Dresselhaus, M. S. Raman Spectroscopy in Graphene. *Phys. Rep.* **2009**, *473*, 51–87.

(27) Chacón-Torres, J. C.; Wirtz, L.; Pichler, T. Raman Spectroscopy of Graphite Intercalation Compounds: Charge Transfer, Strain, and Electron-Phonon Coupling in Graphene Layers. *Phys. Status Solidi* **2014**, *251*, 2337–2355.

(28) Chacón-Torres, J. C.; Wirtz, L.; Pichler, T. Manifestation of Charged and Strained Graphene Layers in the Raman Response of Graphite Intercalation Compounds. *ACS Nano* **2013**, *7*, 9249–9259.

(29) Crowther, A. C.; Ghassaei, A.; Jung, N.; Brus, L. E. Strong Charge-Transfer Doping of 1 to 10 Layer Graphene by NO_2. *ACS Nano* **2012**, *6*, 1865–1875.

(30) Shi, Q.; Dokko, K.; Scherson, D. A. In Situ Raman Microscopy of a Single Graphite Microflake Electrode in a Li^+ -Containing Electrolyte. *J. Phys. Chem. B*, **2004**, *108*, 4789–4793.

(31) Pisana, S.; Lazzeri, M.; Casiraghi, C.; Novoselov, K. S.; Geim, A. K.; Ferrari, A. C.; Mauri, F. Breakdown of the Adiabatic Born-Oppenheimer Approximation in Graphene. *Nat. Mater.* **2007**, *6*, 198–201.

(32) Mohiuddin, T. M. G.; Lombardo, A.; Nair, R. R.; Bonetti, A.; Savini, G.; Jalil, R.; Bonini, N.; Basko, D. M.; Galiotis, C.; Marzari, N.; et al. Uniaxial Strain in Graphene by Raman Spectroscopy: G Peak Splitting, Grüneisen Parameters, and Sample Orientation. *Phys. Rev. B - Condens. Matter Mater. Phys.* **2009**, *79*, 1–8.

(33) Kertesz, M. Changes of Lattice Geometries Upon Charge Transfer. *Mol. Cryst. Liq. Cryst.* **1985**, *126*, 103–110.

(34) Nixon, D. E.; Parry, G. S. The Expansion of the Carbon-Carbon Bond Length in

Potassium Graphites. *J. Phys. C Solid State Phys.* **1969**, *2*, 1732–1741.

(35) Pietronero, L.; Strassler, S. Bond-Length Change as a Tool to Determine Charge Transfer and Electron-Phonon Coupling in Graphite Intercalation Compounds. *Phys. Rev. Lett.* **1981**, *47*, 593–596.

(36) Billaud, D.; Henry, F. X.; Lelaurain, M.; Willmann, P. Revisited Structures of Dense and Dilute Stage II Lithium-Graphite Intercalation Compounds. *J. Phys. Chem. Solids* **1996**, *57*, 775–781.

(37) Guerard, D.; Herold, A. Intercalation of Lithium into Graphite and Other Carbons. *Carbon* **1975**, *13*, 337–345.

(38) Sethuraman, V. A.; Hardwick, L. J.; Srinivasan, V.; Kostecki, R. Surface Structural Disordering in Graphite upon Lithium Intercalation / Deintercalation. *J .Power Sources* **2010**, *195*, 3655–3660.

(39) Kostecki, R.; McLarnon, F.; Microprobe Study of the Effect of Li Intercalation on the Structure of Graphite. *J. Power Sources* **2003**, *119-121*, 550-554

(40) Markevich, E.; Salitra, G.; Levi, M.D.; Aurbach, D. Capacity Fading of Lithiated Graphite Electrodes Studied by a Combination of Electroanalytical Methods, Raman Spectroscopy and SEM. *J. Power Sources* **2005**, 146, 146-150

(41) Hardwick, L. J.; Marcinek, M.; Beer, L.; Kerr, J.B.; Kostecki, R.; An Investigation of the Effect of Graphite Degradation on Irreversible Capacity in Lithium-Ion Cells. *J. Electrochem. Soc.* **2008**, *155*, A442-A447

(42) Chen, C.-F.; Park, C.-H.; Boudouris, B. W.; Horng, J.; Geng, B.; Girit, C.; Zettl, A.; Crommie, M. F.; Segalman, R. A.; Louie, S. G.; et al. Controlling Inelastic Light Scattering Quantum Pathways in Graphene. *Nature* **2011**, *471*, 617–620.

(43) Cohn, A. P.; Share, K.; Carter, R.; Oakes, L.; Pint, C. L. Ultrafast Solvent-Assisted Sodium Ion Intercalation into Highly Crystalline Few-Layered Graphene. *Nano Lett.* **2016**, *16*, 543–548.